Journal of Virology

ADP Ribosylation Factor 1 Plays an Essential Role in the Replication of a Plant RNA Virus

Kiwamu Hyodo, Akira Mine, Takako Taniguchi, Masanori Kaido, Kazuyuki Mise, Hisaaki Taniguchi and Tetsuro Okuno

J. Virol. **2013, 87(1):163. DOI: 10.1128/JVI.02383-12.**
Published Ahead of Print 24 October 2012.

JVI Journals.ASM.org

ADP Ribosylation Factor 1 Plays an Essential Role in the Replication of a Plant RNA Virus

Kiwamu Hyodo,[a] Akira Mine,[a]* Takako Taniguchi,[b] Masanori Kaido,[a] Kazuyuki Mise,[a] Hisaaki Taniguchi,[b] Tetsuro Okuno[a]

Laboratory of Plant Pathology, Graduate School of Agriculture, Kyoto University, Sakyo-ku, Kyoto, Japan[a]; Institute for Enzyme Research, University of Tokushima, Tokushima, Japan[b]

Eukaryotic positive-strand RNA viruses replicate using the membrane-bound replicase complexes, which contain multiple viral and host components. Virus infection induces the remodeling of intracellular membranes. Virus-induced membrane structures are thought to increase the local concentration of the components that are required for replication and provide a scaffold for tethering the replicase complexes. However, the mechanisms underlying virus-induced membrane remodeling are poorly understood. RNA replication of red clover necrotic mosaic virus (RCNMV), a positive-strand RNA plant virus, is associated with the endoplasmic reticulum (ER) membranes, and ER morphology is perturbed in RCNMV-infected cells. Here, we identified ADP ribosylation factor 1 (Arf1) in the affinity-purified RCNMV RNA-dependent RNA polymerase fraction. Arf1 is a highly conserved, ubiquitous, small GTPase that is implicated in the formation of the coat protein complex I (COPI) vesicles on Golgi membranes. Using *in vitro* pulldown and bimolecular fluorescence complementation analyses, we showed that Arf1 interacted with the viral p27 replication protein within the virus-induced large punctate structures of the ER membrane. We found that inhibition of the nucleotide exchange activity of Arf1 using the inhibitor brefeldin A (BFA) disrupted the assembly of the viral replicase complex and p27-mediated ER remodeling. We also showed that BFA treatment and the expression of dominant negative Arf1 mutants compromised RCNMV RNA replication in protoplasts. Interestingly, the expression of a dominant negative mutant of Sar1, a key regulator of the biogenesis of COPII vesicles at ER exit sites, also compromised RCNMV RNA replication. These results suggest that the replication of RCNMV depends on the host membrane traffic machinery.

Eukaryotic positive-strand RNA [(+)RNA] viruses replicate their genomes using membrane-bound replicase complexes, which contain multiple viral and host components. A growing number of host proteins that affect viral RNA replication have been identified using genome-wide and proteomics analyses in several animal and plant viruses (1–13). These host proteins are involved in translation, template selection, and the assembly of the viral replication complex (VRC) on intracellular membranes, which serve as the site of viral RNA replication (14). However, the functions of host proteins remain largely unknown.

The replication compartments of (+)RNA viruses are derived from various cellular organelle membranes, such as the endoplasmic reticulum (ER), mitochondria, chloroplasts, peroxisomes, and the Golgi apparatus (15–17). The formation of viral replication compartments generally involves the emergence of spherules, vesicles, and multivesicular bodies associated with various organelles (15, 17). Although viral proteins play an essential role in the formation of replication compartments containing VRCs, host factors also regulate this process (14, 15, 18). Tomato bushy stunt virus (TBSV) coopts the proteins of the endosomal sorting complexes that are required for transport (ESCRT) to assemble the replicase complex properly on the peroxisome membrane via an interaction with the auxiliary replication protein p33 (19, 20). ESCRT proteins play a major role in the sorting of ubiquitin-modified cargo proteins from the endosomal membrane to the internal vesicles of multivesicular bodies (21). Brome mosaic virus (BMV) replication protein 1a interacts with the reticulon homology proteins (Rhps), which play an important role in the formation of the VRC, probably by regulating membrane curvature (22). Coxsackievirus B3 (CVB3) 3A protein recruits phosphatidylinositol-4-kinase IIIβ (PI4KIIIβ) to the viral replication site to facilitate the formation of the phosphatidylinositol-4-phosphate-enriched compartment, which has a high affinity for the 3D RNA-dependent RNA polymerase (RdRP) (23). Another PI4KIII, PI4KIIIα is required for hepatitis C virus (HCV) replication (1, 9, 12, 24).

Red clover necrotic mosaic virus (RCNMV) is a (+)RNA plant virus that is a member of the genus *Dianthovirus* in the family *Tombusviridae*. The genome of RCNMV consists of RNA1 and RNA2. RNA1 encodes the p27 auxiliary replication protein, the p88 RdRP, and the coat protein (25, 26). RNA2 encodes the movement protein (MP) that is required for viral cell-to-cell movement (27, 28). p27, p88, and host proteins form the 480-kDa replicase complex, which is a key player in the replication of RCNMV RNA (29). p27 and p88 colocalize at the ER membrane (30, 31). RCNMV infection or the expression of p27 is sufficient for inducing a large aggregate structure and the proliferation of the ER membrane (30–32).

We previously found that an affinity-purified RdRP fraction of RCNMV-infected leaves contains several host proteins, including heat shock protein 70 (HSP70), HSP90, and ribosomal proteins (29). To identify further the host factors involved in RCNMV replication, we reevaluated the same affinity-purified RdRP fraction using a MASCOT search and identified ADP ribosylation

Received 5 September 2012 **Accepted** 16 October 2012

Published ahead of print 24 October 2012

Address correspondence to Tetsuro Okuno, okuno@kais.kyoto-u.ac.jp.

* Present address: Akira Mine, Department of Plant Microbe Interactions, Max Planck Institute for Plant Breeding Research, Cologne, Germany.

doi:10.1128/JVI.02383-12

factor 1 (Arf1). Arf1 is a highly conserved, ubiquitous, small GTPase and is implicated in the formation of coat protein complex I (COPI) vesicles on Golgi membranes (33, 34). Brefeldin A (BFA) is a well-known fungal metabolite that inhibits the early secretory pathway (35). BFA inhibits the activation of Arf small GTPases by targeting BFA-sensitive guanine nucleotide-exchange factors (GEFs) (36, 37) via the locking of the abortive Arf-GDP-GEF complex, thereby blocking guanine nucleotide release (38). Arf1 and its BFA-sensitive GEFs are required for the replication of several vertebrate (+)RNA viruses, such as poliovirus, CVB3, mouse hepatitis coronavirus (MHV), and HCV (23, 39–46). However, the direct involvement of Arf1 in RNA replication of plant (+)RNA viruses has not been reported (47).

In this study, using *in vitro* pulldown and bimolecular fluorescence complementation (BiFC) analyses, we show that Arf1 interacts with the RCNMV replication protein p27 within the virus-induced large punctate structures of the ER membrane. We found that BFA treatment reduced the accumulation of the 480-kDa viral replicase complex and RCNMV RNA and decreased p27-induced ER proliferation in RCNMV-infected tobacco BY-2 protoplasts. Similarly, expression of dominant negative Arf1 mutants compromised RCNMV RNA replication in protoplasts. Interestingly, expression of the dominant negative mutant of Sar1, which is a key regulator of the biogenesis of the COPII vesicles at ER exit sites (ERES), also reduced the accumulation of RCNMV RNA. These results suggest that the RNA replication of RCNMV depends on the host membrane traffic machinery.

MATERIALS AND METHODS

Gene cloning and plasmid construction. pUCR1 (48) and pRC2I|G (49) are full-length cDNA clones of RNA1 and RNA2 of an RCNMV Australian strain, respectively. pB1TP3, pB2TP5, and pB3TP8 are full-length cDNA clones of RNA1, RNA2, and RNA3 of the BMV M1 strain, respectively (50) (generous gift from Paul Ahlquist). The constructs described previously used in this study include pBICp27-HA:cYFP (where HA is hemagglutinin and cYFP is a C-terminal fragment of the yellow fluorescent protein) (32), pBICHA:cYFP (32), pBICmyc:nYFP (where nYFP is an N-terminal fragment of YFP) (32), pBICp19 (48), pBICER:mCherry (51), pUBp27-FLAG (52), pUBp27-HA (32), pUBp88-HA (32), pCOLDp27 (57), pCOLDp27N (57), pCOLDp27C (57), pCOLDGSTp27 (where GST is glutathione *S*-transferase) (57), pR1-Luc-R1 (where Luc is luciferase) (53), pLUCpA60 (54), and pSP64-RLUC (54). pUC118 was purchased from TaKaRa Bio Inc. (Shiga, Japan). *Escherichia coli* DH5α was used for the construction of all plasmids. All plasmids constructed in this study were verified by sequencing. The primers used in this study are listed in Table 1.

RNA extraction from *Nicotiana benthamiana* leaves, tobacco (*Nicotiana tabacum*) BY-2 cells, or *Arabidopsis thaliana* (Col-0) leaves was performed using an RNeasy Plant Mini Kit (Qiagen, Hilden, Germany). Reverse transcription-PCR (RT-PCR) was catalyzed by Superscript III reverse transcriptase (Invitrogen) using oligo(dT) (32).

pTVNbArf1. A 399-bp Arf1 cDNA fragment (55) was amplified from cDNA derived from *N. benthamiana* (NbArf1) RNA using primers 1 and 2. The generated PCR product was then cloned in the antisense orientation into the SmaI site of pTV00 (56).

pBYLNtArf1. The coding sequence of Arf1 was amplified from cDNA derived from *N. tabacum* BY-2 (NtArf1) RNA using primers 3 and 4. The amplified DNA was digested with AscI and inserted into pBYL2 (29) that had been cut with the same restriction enzyme.

pColdGST-NtArf1. The sequence of NtArf1 was amplified from pBYLNtArf1 using primers 5 and 6. The amplified DNA was digested with KpnI and inserted into pColdGST (57) that had been cut with the same restriction enzyme.

TABLE 1 List of primers used in this study

Primer no.	Sequence
1	CTGTGCTGCTTGTTTTTGCT
2	CTTCGTTTACAAATTTATG
3	GGCGCGCCATGGGGCTGTCTTTCGGCAAACTTTTCAGTCG
4	GGCGCGCCCTATGCCTTGTTTGAAATATTGTTCGAAAGCC
5	CGGGGTACCATGGGGCTGTCTTTCGGCAAACTTTTCAGTCGCC
6	CGGGGTACCCTATGCCTTGTTTGAAATATTGTTCGAAAGCC
7	AGAGGCCTACGGGGATCCAAGGAGATATAACAATGGGGCTGTCT
8	CTACTTGTCATCGTCGTCCTTGTAATCTGCCTTGTTTGAAATAT
9	GATTACAAGGACGACGATGACAAGTAGTAAGAATTCCGGGTACC
10	CAGGAAACAGCTATGACCATG
11	GCTCGGTACCATGGGGCTGTCTTTCGGCAAACTTTTCAGTCGCC
12	AGCTTCTGCTCCATGCCCCCTGCCTTGTTTGAAATATTGTTCGA
13	TTTCAAACAAGGCAGGGGGCATGGAGCAGAAGCTGATCAGCGAG
14	CGGGGATCCCCGTAGGCCTCTAGGCCATGATATAGACGTTGTGG
15	GGCGCGCCATGGGGTTGTCATTCGGAAAGTTGTTCAGC
16	GGCGCGCCCTATGCCTTGCTTGCGATGTTGTTGGAGAGCC
17	GGGGATCCGATGGGGTTGTCATTCGGAAAGTTGTTCAGCAGGC
18	GGGGTACCCGGAATTCTTACTATGCCTTGCTTGCGATGTTGTTG
19	AAGGGATGACGCACAATCCC
20	TGATGATGATGATGATGCATTGCCTTGCTTGCGATGTTGTTGGA
21	ACAACATCGCAAGCAAGGCAATGCATCATCATCATCATCATGTG
22	AGCTTGTAGAGGATAGTGTTCTTACCAGCAGCATCGAGACCAAC
23	GTCTCGATGCTGCTGGTAAGAACACTATCCTCTACAAGCTCAAA
24	AATGGACGGATCTTGTCTAGACCCCCAACATCCCACACGGTGAA
25	CCGTGTGGGATGTTGGGGGTCTAGACAAGATCCGTCCATTGTGG
26	GGCGCGCCATGTTCTTGTTCGATTGGTTCTACGG
27	GGCGCGCCTTAGTTGATGTACTGAGAGAGCCATTTGAATCC
28	GGGGATCCGATGTTCTTGTTCGATTGGTTCTACGGAATCTTAGC
29	GGGGTACCCGGAATTCTTATTAGTTGATGTACTGAGAGAGCCAT
30	TGATGATGATGATGATGCATGTTGATGTACTGAGAGAGCCATTT
31	GGCTCTCTCAGTACATCAACATGCATCATCATCATCATCATGTG
32	ACCCTACGAGCAATCTGAAGACCACCCAAATCAAAAGCCTTGAA
33	AGGCTTTTGATTTGGGTGGTCTTCAGATTGCTCGTAGGGTTTGG
34	AGAGGCCTACGGGGGGATCCGATGAATATCTTTAGATTTGCTGG
35	CCCTTGCTCACCATGCCCCCAAAATCCTCAAGGGATTTGAACCC
36	CCCTTGAGGATTTTGGGGGCATGGTGAGCAAGGGCGAGGAGGAT
37	CCTGTCGATGTACTCGAGAAGGTGGCGTTT
38	TCCTCGCCCTTGCTCACCATGCCCCCTCGGGCTTTGATTAGATC
39	TAATCAAAGCCCGAGGGGGCATGGTGAGCAAGGGCGAGGAGGAT
40	CGGGATCCAAGGAGATATAACAATG
41	CTCCTCGCCCTTGCTCACGAATTCGGCCGAGGATAA
42	TTATCCTCGGCCGAATTCGTGAGCAAGGGCGAGGAG
43	GGGGTACCTTAAAGCTCATCATGCTTGTACAGCTCGTCCAT
44	AATGACAGAGACCGTGTTGTTGA
45	ACAGCATCCCGAAGCTCATC
46	CCTCTGCAGTTGCCACC
47	CCTGTGGGTATGCCTTCTTC

pColdNtArf1-FLAG. PCR fragments from pBYLNtArf1 were amplified using primers 7 and 8 and primers 9 and 10. Then, a recombinant PCR product was amplified from the mixture of these fragments using primers 7 and 10. The amplified fragment was digested with BamHI and KpnI and inserted into the corresponding region of pUBP35 (48) to generate pUBNtArf1-FLAG. PCR fragments from pUBNtArf1-FLAG were amplified using primers 5 and 10. The amplified DNA was digested with KpnI and inserted into the corresponding region of pCOLDI (TaKaRa Bio Inc.).

pBICNtArf1-myc:nYFP. The sequence of NtArf1 was amplified from pBYLNtArf1 using primers 7 and 12. The sequence of the myc-tagged N-terminal half of YFP was amplified from pBICmyc:nYFP (32) using primers 13 and 14. Then, a recombinant PCR product was amplified from the mixture of these fragments using primers 7 and 14. The amplified

fragment was digested with BamHI and inserted into the corresponding region of pBICP35 (48).

pBYLAtArf1. The coding sequence of Arf1 was amplified from cDNA derived from *A. thaliana* (AtArf1) RNA using primers 15 and 16. The amplified DNA was digested with AscI and inserted into pBYL2 that had been cut with the same restriction enzyme.

pUBAtArf1. The sequence of AtArf1 was amplified from pBYLAtArf1 using primers 17 and 18. The amplified DNA was digested with BamHI and KpnI and inserted into the corresponding region of pUBP35.

pUBAtArf1-GFP. The sequence of AtArf1 was amplified from pUBAtArf1 using primers 19 and 20. The sequence of a green fluorescent protein (GFP) gene was amplified from pUBsGFP (where sGFP is synthetic GFP) (51) using primers 10 and 21. Then, a recombinant PCR product was amplified from the mixture of these fragments using primers 10 and 19. The amplified DNA was digested with StuI and KpnI and inserted into the corresponding region of pUBP35.

pUBAtArf1-T31N. PCR fragments from pBYLAtArf1 were amplified using primers 17 and 22 and primers 18 and 23. Then, a recombinant PCR product was amplified from the mixture of these fragments using primers 17 and 18. The amplified fragment was digested with BamHI and KpnI and inserted into the corresponding region of pUBP35.

pUBAtArf1-Q71L. PCR fragments from pBYLAtArf1 were amplified using primers 17 and 24 and primers 18 and 25. Then, a recombinant PCR product was amplified from the mixture of these fragments using primers 17 and 18. The amplified fragment was digested with BamHI and KpnI and inserted into the corresponding region of pUBP35.

pBYLAtSar1. The coding sequence of Sar1 was amplified from cDNA derived from *A. thaliana* (AtSar1) RNA using primers 26 and 27. The amplified DNA was digested with AscI and inserted into pBYL2 that had been cut with the same restriction enzyme.

pUBAtSar1. The sequence of AtSar1 was amplified from pBYLAtSar1 using primers 28 and 29. The amplified DNA was digested with BamHI and KpnI and inserted into the corresponding region of pUBP35.

pUBAtSar1-GFP. The sequence of AtSar1 was amplified from pUBAtSar1 using primers 19 and 30. The sequence of GFP was amplified from pUBsGFP using primers 10 and 31. Then, a recombinant PCR product was amplified from the mixture of these fragments using primers 10 and 19. The amplified DNA was digested with StuI and KpnI, and inserted into the corresponding region of pUBP35.

pUBAtSar1-H74L. PCR fragments from pBYLAtSar1 were amplified using primers 28 and 32 and primers 29 and 33. Then, a recombinant PCR product was amplified from the mixture of these fragments using primers 28 and 29. The amplified fragment was digested with BamHI and KpnI and inserted into the corresponding region of pUBP35.

pUBAtErd2-GFP. The sequence of C-terminally GFP-fused AtErd2 was amplified from pMT121-AtErd2-sGFP (58) (generous gift from Akihiko Nakono) using primers 10 and 34. The amplified DNA was digested with StuI and KpnI, and inserted into the corresponding region of pUBP35.

pUBp27-mCherry. A PCR fragment from pUBp27 (48) was amplified using primers 19 and 35, and a PCR fragment from pBICER-mCherry (51) was amplified using primers 10 and 36. Then, a recombinant PCR product was amplified from the mixture of these fragments using primers 10 and 19. The amplified fragment was digested with BamHI and KpnI and inserted into the corresponding region of pUBP35.

pUBp88-mCherry. A PCR fragment from pUBp88 (48) was amplified using primers 37 and 38, and a PCR fragment from pUBp27-mCherry was amplified using primers 10 and 39. Then, a recombinant PCR product was amplified from the mixture of these fragments using primers 10 and 37. The amplified fragment was digested with XhoI and KpnI and inserted into the corresponding region of pUBp88.

pUBER-GFP. A PCR fragment from pUCmGFP5-ER (59) (generous gift from Joan Wellink) was amplified using primers 40 and 41, and a PCR fragment from pUBsGFP was amplified using primers 42 and 43. Then, a recombinant PCR product was amplified from the mixture of these fragments using primers 40 and 43. The amplified fragment was digested with BamHI and KpnI and inserted into the corresponding region of pUBP35.

Identification of Arf1. Protein identification based on in-gel digestion and liquid chromatography-tandem mass spectrometry (LC-MS/MS) was carried out as described previously (60). Data obtained using a hybrid Fourier transform-ion cyclotron resonance (FT-ICR) mass spectrometer (LTQ-FT; Thermo, San Jose, CA) were processed using the Mascot Distiller software (version 2.3.2; Matrix Science, United Kingdom), and the peak lists obtained were used to search the NCBI nonredundant protein database (NCBInr 20120416) using the Mascot search engine (version 2.3; Matrix Science, United Kingdom). The taxonomy was restricted to Viridiplantae (green plants). The mass tolerances were set to ±2 ppm for MS and ±0.25 Da for MS/MS analyses.

Antibodies. Rabbit anti-p27 antiserum (48) was used at 1:100 for immunofluorescence labeling. Mouse monoclonal antibodies were used at the following dilutions: for immunoblotting, anti-FLAG M2 antibody (F3165; Sigma-Aldrich) at 1:10,000 and, for immunofluorescence labeling, anti-bromodeoxyuridine (BrdU) antibody (B2531; Sigma-Aldrich) at 1:100. A rat anti-HA antibody (1867423; Roche) was used at 1:2,000 for immunoblotting. The secondary antibodies were goat anti-rabbit conjugated to Alexa Fluor 488 (A-11008; Molecular Probes) at 1:100 and goat anti-mouse conjugated to Alexa Fluor 594 (A-21125; Molecular Probes) at 1:100 for immunofluorescence labeling. For immunoblotting, a horseradish peroxidase-conjugated anti-mouse IgG antibody (074-1806; KPL) and alkaline phosphatase-conjugated anti-rat IgG antibody (sc-2021; Santa Cruz Biotechnology Inc.) were used to visualize the antigen-antibody complexes.

Expression and purification of recombinant proteins. The expression and purification of the recombinant N-terminally 6×His- and C-terminally FLAG-tagged p27 protein were performed as described previously (57). For expression of NtArf1, *E. coli* strain BL21(DE3) transformed with pColdNtArf1-FLAG was grown overnight at 37°C in Luria Broth (LB) medium containing ampicillin (50 μg/ml). The overnight culture (2 ml) was added to 100 ml of LB medium containing ampicillin (50 μg/ml). After the culture was incubated for 1 h at 37°C and subsequently for 30 min at 15°C, protein expression was induced by the addition of 0.3 mM isopropyl-β-D-thiogalactopyranoside (IPTG), followed by incubation at 15°C for 24 h. The induced cells were harvested by centrifugation at 5,000 × *g* for 5 min, resuspended in 1 ml of His buffer (100 mM HEPES, pH 7.5, 300 mM NaCl) supplemented with 30 mM imidazole, and sonicated on ice. Subsequently, Triton X-100 was added at a final concentration of 0.5% and centrifuged at 21,000 × *g* at 4°C for 10 min. The supernatant was added to the 50-μl bed volume of equilibrated Ni-nitrilotriacetic acid (NTA)-agarose (Qiagen, Hilden, Germany) and incubated at 4°C for 1 h with gentle rotation. The resin was washed three times with 1 ml of His buffer supplemented with 30 mM imidazole and eluted with TBS buffer (50 mM Tris-HCl, pH 7.5, 150 mM NaCl, 2 mM dithiothreitol [DTT]) containing 15% glycerol and 250 mM imidazole. The concentration of purified protein was measured using a Coomassie Protein Assay Kit (Thermo Fisher Scientific, Waltham, MA). The purified protein was subjected to sodium dodecyl sulfate-polyacrylamide gel electrophoresis (SDS-PAGE) and visualized with Coomassie brilliant blue R-250 to check its purity.

GST pulldown assay. *E. coli* BL21(DE3) transformed with plasmids containing the prefix pColdGST was grown overnight at 37°C in LB medium containing ampicillin (50 μg/ml). The overnight cultures of the transformed *E. coli* were diluted 1:50 in LB medium containing ampicillin (50 μg/ml). After the cultures were incubated at 37°C for 1.5 h and subsequently at 15°C for 30 min, protein expression was induced by addition of 0.3 mM IPTG. The cells were cultured for 2 h. The induced cells were harvested by centrifugation at 5,000 × *g* for 5 min. Cells collected from 5 ml of medium were resuspended in 500 μl of TBS buffer and sonicated on ice to disrupt the cells. After sonication, Triton X-100 was added at a final concentration of 0.5% and centrifuged at 21,000 × *g* at 4°C for 10 min. The supernatant was added to a 12.5-μl bed volume of equilibrated glu-

tathione-Sepharose 4B (GE Healthcare, Little Chalfont, Buckinghamshire, United Kingdom) and incubated at 4°C for 1 h with gentle rotation. The resin was washed three times with 1 ml of TBS buffer supplemented with 0.5% Triton X-100. After the washing step, the resin was incubated at 4°C for 2 h in 200 μl of TBS buffer containing 1 μg of His-p27-FLAG or His-NtArf1-FLAG. After incubation, the resin was washed three times with 500 μl of TBS buffer. The bound proteins were eluted by the addition of Laemmli sample buffer (61), followed by incubation at 95°C for 3 min. Protein samples were subjected to immunoblotting using an anti-FLAG antibody.

RNA preparation. RCNMV RNA1 and RNA2 were transcribed from SmaI-linearized pUCR1 and pRC2|G, respectively, using T7 RNA polymerase (TaKaRa Bio, Inc.). BMV RNAs were transcribed from EcoRI-linearized pB plasmids using T7 RNA polymerase and capped with a ScriptCapm^{7}G capping system (Epicentre Biotechnology). R1-Luc-R1 was synthesized from an SmaI-linearized plasmid. Luc mRNA and R-Luc mRNA were transcribed from EcoRI-linearized pLUCpA60 and pSP64-RLUC, respectively, and capped using the ScriptCapm^{7}G capping system. All transcripts were purified with a Sephadex G-50 fine column (Amersham Pharmacia Biotech). RNA concentration was determined spectrophotometrically, and its integrity was verified by agarose gel electrophoresis.

***Agrobacterium* infiltration.** The plasmids containing the prefixes pBIC and pTV were introduced by electroporation into *Agrobacterium tumefaciens* GV3101 (pMP90) and *A. tumefaciens* GV3101 (pSoup), respectively. *Agrobacterium* suspensions were mixed at final optical density at 600 nm (OD_{600}) of 0.2 each for BiFC experiments and an OD_{600} of 0.5 each for gene silencing experiments. The mixture was infiltrated into *N. benthamiana* leaves as described previously (32).

BiFC experiment. Appropriate combinations of YFP fragment-fused or fluorescent protein-fused proteins were expressed in *N. benthamiana* leaves by *Agrobacterium* infiltration. The fluorescence of YFP and mCherry was visualized at 3 days postinfiltration (dpi).

Confocal microscopy. Tobacco BY-2 protoplasts were inoculated with plasmids expressing fluorescent protein-fused proteins (10 μg each) and incubated at 17°C for 16 h as described previously (52). The fluorescence of GFP and mCherry was visualized using an Olympus FluoView FV500 confocal microscope (Olympus Optical Co., Tokyo, Japan) as described previously (27). To test the effect of BFA, the inoculated protoplasts were incubated with dimethyl sulfoxide (DMSO; Sigma-Aldrich) or 10 μg/ml BFA (Wako, Osaka, Japan) for an additional 2 h before observation. All images shown are from a 1-μm single optical section and were processed using Adobe Photoshop CS3 software.

Silencing of *Arf1* in *N. benthamiana* plants. Appropriate combinations of silencing vectors were expressed via *Agrobacterium* infiltration in 3- to 4-week-old *N. benthamiana* plants as described previously (56). At 7 days postinfiltration (dpi), the leaves located above the infiltrated leaves were inoculated with *in vitro* transcribed RNA1 and RNA2 (1 μg each). At 2 days after inoculation, three inoculated leaves from three different plants infected with same inoculum were pooled, and total RNA was extracted using PureLink (Invitrogen), treated with RQ1 RNase-free DNase (Promega, Madison, WI), purified by phenol-chloroform and chloroform extractions, and precipitated with ethanol. Viral RNAs were detected by Northern blotting, as described previously (32). The mRNA levels of *NbArf1* were examined by RT-PCR using primers 44 and 45. As a control to show the equal amounts of cDNA templates in each reaction mixture, the ribulose 1,5-biphosphate carboxylase small subunit gene (*RbcS*), a gene that is constitutively expressed, was amplified by RT-PCR using primers 46 and 47.

Replication assay. Tobacco BY-2 protoplasts were inoculated with RCNMV RNA1 (1.5 μg) and RNA2 (0.5 μg) and incubated with 10 μg/ml BFA at 17°C for 16 h. For the BMV replication assay, tobacco BY-2 protoplasts inoculated with BMV RNA1, RNA2, and RNA3 (1.5 μg each) were incubated with 10 μg/ml BFA at 17°C or 22°C for 20 h. For transient expression of Arf1, tobacco BY-2 protoplasts inoculated with plasmids expressing RNA1 and RNA2 (1 μg each), together with plasmids expressing Arf1 or its GTP- or GDP-fixed mutants (18 μg each), were incubated at 17°C for 24 h.

Total RNA was extracted and subjected to Northern blotting, as described previously (52). Each experiment was repeated at least three times using different batches of protoplasts.

Luciferase assay. Tobacco BY-2 protoplasts inoculated with reporter RNAs were incubated with 10 μg/ml BFA at 17°C for 6 h. Luciferase assays were performed using a Dual-Luciferase Assay System (Promega, Madison, WI), as described previously (54). Each experiment was repeated at least three times using different batches of protoplasts.

BN-PAGE analyses. Plasmids expressing p27-HA and p88-HA were transfected to BY-2 protoplasts in the presence of RNA2. After 16 h of incubation at 17°C, protoplasts were harvested and resuspended in TR buffer (62) supplemented with 1% Triton X-100. Subsequently, protoplasts were disrupted freezing and thawing and centrifuged at 21,000 × *g* at 4°C for 10 min to remove cell debris and unbroken cells. The supernatants were subjected to Blue native (BN)- and SDS-PAGE followed by immunoblotting using an anti-HA antibody.

Coimmunopurification. Plasmids expressing p27-HA and p88-HA were transfected with either p27 or p27-FLAG into BY-2 protoplasts in the presence of RNA2. After 16 h of incubation at 17°C, protoplasts were harvested and resuspended in TR buffer supplemented with 1% Triton X-100. Subsequently, protoplasts were disrupted by freezing and thawing and centrifuged at 21,000 × *g* at 4°C for 10 min to remove cell debris and unbroken cells. The supernatants were subjected to 12.5 μl of bed volume of ANTI-FLAG M2-Agarose Affinity Gel (Sigma-Aldrich) and incubated for 2 h with gentle mixing at 4°C. The resin was washed two times with 200 μl of TR buffer supplemented with 0.5% Triton X-100. The bound proteins were eluted by addition of Laemmli sample buffer, followed by incubation at 95°C for 3 min. Protein samples were subjected to SDS-PAGE, followed by immunoblotting using the appropriate antibodies.

Fractionation assay. Plasmids expressing p27-HA and p88-HA were transfected into BY-2 protoplasts in the presence of RNA2. After 16 h of incubation at 17°C, protoplasts were harvested and resuspended in 500 μl of TR buffer. Subsequently, protoplasts were disrupted by freezing and thawing and centrifuged at 4,000 × *g* at 4°C for 10 min. The cell extracts obtained were further centrifuged at 21,000 × *g* at 4°C for 10 min to separate the supernatant and pellet fractions. The pellet fraction was resuspended in 50 μl of TR buffer supplemented with 0.5% Triton X-100. Aliquots of each fraction were subjected to immunoblotting using an anti-HA antibody.

***In vivo* RNA labeling.** Tobacco BY-2 protoplasts (approximately 3 × 10^5 cells) were inoculated with RNA1 (1.5 μg) and RNA2 (0.5 μg), as described previously (52). After 14 h, actinomycin D (Sigma-Aldrich) (10 μg/ml) was added, and protoplasts were incubated for 1 h to block RNA transcription from cellular DNA-dependent RNA polymerases. Subsequently, 2 mM 5-bromouridine 5′-triphosphate (BrUTP; Sigma-Aldrich) was added, and protoplasts were incubated for an additional 3 h. Protoplasts were placed on a cover slide pretreated with poly-L-lysine. The reaction was stopped by the addition of PHEM buffer (60 mM PIPES [piperazine-*N*,*N*′-bis(2-ethanesulfonic acid)], 25 mM HEPES, 2 mM $MgCl_2$, 5 mM EGTA, pH 6.9) containing 3% formaldehyde and 2.5% DMSO. After 15 min of incubation, the slide was washed three times with PHEM buffer and incubated in ice-cold methanol for 10 min. The samples were incubated with the primary antibodies for 1 h and washed three times with PHEM buffer. Then, they were incubated with Alexa Fluor 488- and 594-conjugated secondary antibodies for 1 h and washed three times with PHEM buffer.

RESULTS

Arf1 interacts directly with p27. We reevaluated the data obtained by LC-MS/MS analyses of the affinity-purified RdRP membrane fraction (29) and found that Arf1 was present in the fraction that coimmunoprecipitated with FLAG-tagged p27 (Table 2).

TABLE 2 The host proteins copurified with p27-FLAG

Gene identification no.	Description
gi|1703374	ADP ribosylation factor 1
gi|10798648	Putative DnaJ protein
gi|175363751	Elongation factor 1 gamma-like protein
gi|120661	Glyceraldehyde-3-phosphate dehydrogenase A
gi|120665	Glyceraldehyde-3-phosphate dehydrogenase B

This result led us to perform a GST pulldown assay to determine whether Arf1 interacts with p27. Bacterially expressed and purified p27 with an N-terminal 6×His tag and C-terminal FLAG tag (His-p27-FLAG) (57) was incubated with N-terminally GST-fused Arf1 (GST-Arf1) or GST captured on glutathione-bound beads. Immunoblot analyses using an anti-FLAG antibody showed that His-p27-FLAG was pulled down by GST-Arf1 but not by GST (Fig. 1A), indicating that p27 binds to Arf1 *in vitro*. A parallel GST pulldown assay using purified N-terminally 6×His-tagged and C-terminally FLAG-tagged Arf1 (His-Arf1-FLAG) (Fig. 1B) and glutathione resin-bound N-terminally GST-fused p27 or its truncated proteins (Fig. 1C) confirmed a p27-Arf1 interaction *in vitro* (Fig. 1D). Moreover, His-Arf1-FLAG was pulled down more efficiently by the C-terminal half of p27 than by the N-terminal half of p27, suggesting that Arf1 interacted preferentially with the C-terminal region of p27 (Fig. 1D).

To further test the interaction between Arf1 and p27 *in vivo*, we performed a BiFC experiment in *N. benthamiana* epidermal cells. Arf1 that was fused to the N-terminal half of yellow fluorescent

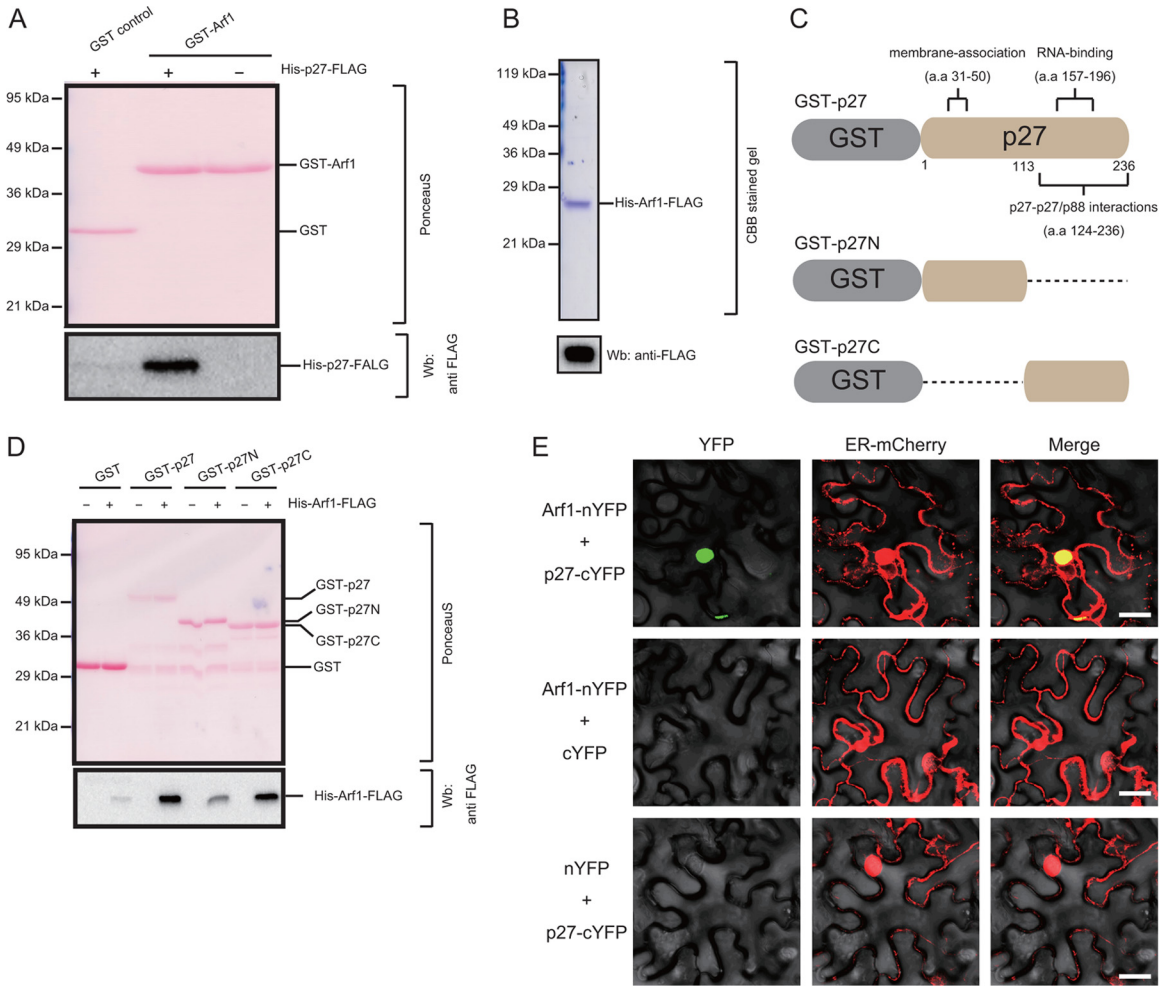

FIG 1 p27 interacts with Arf1 *in vitro* and *in vivo*. (A) Glutathione resin-bound GST-fused Arf1 (GST-Arf1) was incubated with the purified recombinant His-p27-FLAG. After a washing step, pulled down complexes were subjected to SDS-PAGE and analyzed by Western blotting (Wb) using an anti-FLAG antibody. After detection, the proteins separated on the membrane were visualized using Ponceau S staining. (B) SDS-PAGE analyses of purified His-Arf1-FLAG expressed in *E. coli*. The purified protein (1 μg) was visualized using Coomassie brilliant blue (CBB) staining (top panel) and analyzed by immunoblotting using an anti-FLAG antibody (bottom panel). (C) Schematic representation of the deleted derivatives of GST-p27. The deletions are represented as dotted lines. The locations of known functional domains in wild-type p27 are depicted. aa, amino acids. (D) Glutathione resin-bound GST-p27 or its derivatives were incubated with purified recombinant His-Arf1-FLAG. After a washing step, pulled down complexes were subjected to SDS-PAGE and analyzed by immunoblotting using an anti-FLAG antibody. After detection, the proteins separated on the membrane were visualized using Ponceau S staining. (E) Bimolecular fluorescence complementation analyses of the interactions between p27 and Arf1. p27 fused to the C-terminal half of YFP, at the C terminus (p27-cYFP), was expressed together with Arf1 fused to the other half of YFP, at the C terminus (Arf1-nYFP), in the presence of ER-mCherry and of an RNA-silencing suppressor of the TBSV, p19, in *N. benthamiana* leaves via *Agrobacterium* infiltration. The fluorescence of the reconstructed YFP and ER-mCherry in all agroinfiltrated leaves was visualized using confocal microscopy 3 days after agroinfiltration. The panels on the right show the merging of mCherry and YFP (yellow). Scale bar, 20 μm.

protein (YFP) at the C terminus (Arf1-nYFP) and p27 that was fused to the C-terminal half of YFP at the C terminus (p27-cYFP) were expressed together with mCherry containing an ER targeting signal (ER-mCherry) and the TBSV silencing suppressor p19 in *N. benthamiana* via agroinfiltration. At 3 dpi, fluorescence was observed using confocal laser scanning microscopy (CLSM). YFP fluorescence was reconstituted in the presence of Arf1-nYFP and p27-cYFP (Fig. 1E, top left panel). YFP fluorescence merged well with ER-mCherry fluorescence in the large punctate structures (Fig. 1E, top panels), a characteristic feature of morphological ER changes induced by p27 or RCNMV infection (30–32). Negligible or no YFP fluorescence was detected in control experiments (Fig. 1E, middle and bottom panels). These results indicate that p27 interacts directly with Arf1 at the p27-induced modified ER membrane.

Arf1 is recruited from the Golgi apparatus to the RCNMV replication site by p27. In plant cells, Arf1 is localized at the Golgi apparatus (63–66). However, the Arf1-p27 interaction occurred at the ER in *N. benthamiana* epidermal cells (Fig. 1E). This result prompted us to test the possibility that p27 recruits Arf1 from the Golgi apparatus to the ER membrane, which is a putative site of RCNMV replication (31). First, we examined whether p27 colocalizes with Arf1. For this, a plasmid expressing C-terminally GFP-fused Arf1 (Arf1-GFP) was cotransfected with a plasmid expressing C-terminally mCherry-fused p27 (p27-mCherry) or a control plasmid into tobacco BY-2 protoplasts, and fluorescence was observed via CLSM after 16 h of incubation. In the absence of p27-mCherry, Arf1-GFP fluorescence was observed as small punctate structures throughout the cell, a typical fluorescence pattern of Golgi compartment-localized proteins (Fig. 2A) (67, 68). Interestingly, however, in the presence of p27-mCherry, the small punctate fluorescence pattern of Arf1-GFP was dramatically reduced, and Arf1-GFP fluorescence was observed as large aggregate structures located around the nucleus (Fig. 2B, left panel). Moreover, these aggregated structures colocalized with p27-mCherry (Fig. 2B, middle and right panels). Similar results were obtained for Erd2-GFP (data not shown), a well-established *cis*-Golgi marker (69). Expression of C-terminally mCherry-fused p88 (p88-mCherry) also affected the distribution pattern of Arf1-GFP, but large aggregated structures of Arf1-GFP were not observed (Fig. 2C). p27-mCherry and p88-mCherry efficiently supported the replication of RNA2 (data not shown). It should be noted that both mCherry-fused p27 and p88 colocalized with the ER marker protein in BY-2 protoplasts (see Fig. 5; also data not shown).

Arf1 plays an important role in RCNMV RNA replication. To investigate whether Arf1 is required for infection of host plants with RCNMV, we downregulated Arf1 using *Tobacco rattle virus* (TRV)-based virus-induced gene silencing in *N. benthamiana* plants. A TRV vector harboring a partial fragment of NbArf1 (TRV:NbArf1) was expressed via *Agrobacterium*-mediated expression. An empty TRV vector (TRV:00) was expressed as a control. Newly developed leaves were inoculated with RCNMV RNA1 and RNA2 at 7 dpi. Two days after inoculation, three inoculated leaves from three different plants were harvested and mixed, and total RNA was extracted. Semiquantitative RT-PCR analyses confirmed the specific reduction of NbArf1 mRNA in plants infiltrated with TRV:NbArf1 (Fig. 3A). Northern blot analyses showed that the accumulation of RCNMV RNA was reduced 10-fold in NbArf1-silenced plants compared with control plants (Fig. 3A), suggesting that Arf1 plays a positive role in RCNMV infection.

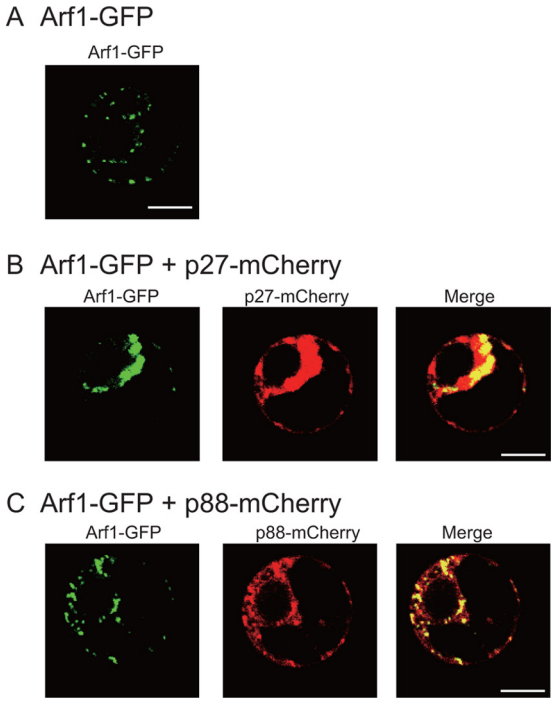

FIG 2 Colocalization of Arf1 with RCNMV replicase proteins. A plasmid expressing C-terminally GFP-fused Arf1 (Arf1-GFP) was cotransfected with plasmids expressing C-terminally mCherry-fused p27 (p27-mCherry) or with an empty vector into tobacco BY-2 protoplasts. Fluorescence was observed after 16 h of incubation. (A) In the absence of p27-mCherry, Arf1-GFP fluorescence was observed as small punctate structures throughout the cell. (B) Arf1-GFP fluorescence was observed as large aggregate structures in the presence of p27-mCherry. (C) Arf1-GFP fluorescence in the presence of p88-mCherry. Fluorescence was visualized by confocal microscopy. The merging of green and red fluorescence is shown in yellow. Scale bar, 5 μm.

It has been well documented that BFA inhibits the secretion of proteins from the Golgi apparatus back to the ER (35) via inhibition of the nucleotide-exchange reaction of Arf proteins (38). To investigate whether Arf1 plays a role in RCNMV RNA replication, we tested the effect of BFA on the accumulation of RCNMV RNA replication in a single cell. Tobacco BY-2 protoplasts were inoculated with RCNMV RNA1 and RNA2 and incubated for 16 h in the presence or absence of BFA. Northern blot analyses showed that the accumulation of viral RNAs was reduced 5- to 10-fold in the presence of BFA (Fig. 3B). BFA did not affect the accumulation of rRNA (Fig. 3B, bottom panel). Moreover, BFA had a negligible effect on the accumulation of BMV RNA in BY-2 protoplasts (Fig. 3C). These results indicate that the inhibitory effect of BFA on RCNMV RNA replication was not due to its nonspecific toxicity and that the inhibition of Arf function by BFA specifically affects RCNMV RNA replication. Next, to investigate whether the inhibitory effect of BFA is due to the inhibition of Arf1 GEF activity, we tested the effects of constitutive-negative (Arf1 with a T31N mutation [Arf1-T31N]) and constitutive-active (Arf1-Q71L) Arf1 mutants on RCNMV RNA replication. Arf1-T31N is a GDP-restricted Arf1 mutant that impairs the normal COPI function and inhibits the formation of ERES (64–66, 70). Arf1-Q71L is a GTP-restricted Arf1 mutant that inhibits the vacuolar sorting of sporamin in tobacco BY-2 cells (66). Tobacco BY-2 protoplasts were transfected with plasmids expressing wild-type Arf1, Arf1-

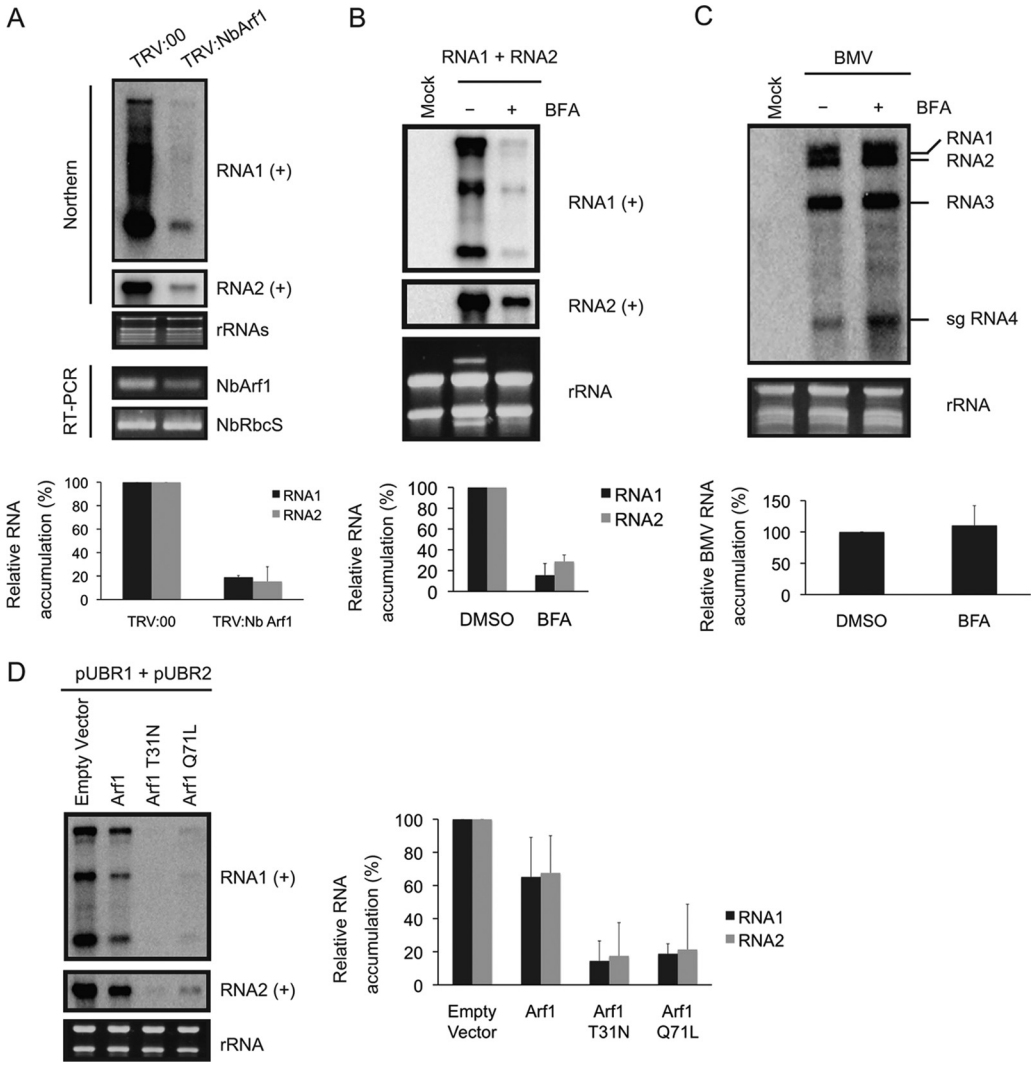

FIG 3 (A) Knockdown of Arf1 mRNA levels via gene silencing inhibits the accumulation of RCNMV RNAs in *N. benthamiana* plants. The tobacco rattle virus (TRV) vector harboring a partial fragment of *N. benthamiana* Arf1 (TRV:NbArf1) was expressed in *N. benthamiana* via *Agrobacterium* infiltration. The empty TRV vector (TRV:00) was used as a control. The newly developed leaves were inoculated with RCNMV RNA1 and RNA2 7 days after agroinfiltration. Total RNA was extracted from the mixture of three independent inoculated leaves 2 days after inoculation. Accumulation of RCNMV RNAs was analyzed by Northern blotting. Ethidium bromide-stained ribosomal RNAs (rRNAs) are shown below the Northern blots, as loading controls. Arf1 mRNA levels were assessed by RT-PCR using primers that allow the amplification of the region of Arf1 that is not present in TRV:NbArf1. RT-PCR results for the RbcS gene demonstrated that equal amounts of total RNA were used for the RT and showed equivalent efficiency of the RT reaction in the samples. (B) An inhibitor of Arf1 impairs RCNMV RNA replication in a single cell. Tobacco BY-2 protoplasts were inoculated with *in vitro* transcribed RNA1 and RNA2. The inoculated protoplasts were incubated at 17°C for 16 h in the presence of 10 μg/ml BFA. (C) An inhibitor of Arf1 does not impair BMV RNA replication in a single cell. Tobacco BY-2 protoplasts were inoculated with *in vitro* transcribed BMV RNAs. The inoculated protoplasts were incubated at 17°C for 20 h in the presence of 10 μg/ml BFA. (D) Dominant negative mutants of Arf1 inhibit RCNMV replication. Tobacco BY-2 protoplasts were transfected with plasmids expressing either wild-type Arf1, Arf1-T31N, or Arf1-Q71L together with pUBRC1 and pUBRC2, which encode RNA1 and RNA2, respectively, under the control of the cauliflower mosaic virus 35S promoter. The inoculated protoplasts were incubated at 17°C for 24 h. Total RNA was analyzed by Northern blotting. Ethidium bromide-stained rRNAs were used as loading controls and are shown below the Northern blots. The accumulated levels of RCNMV or BMV RNAs from three separate experiments were quantified using the Image Gauge program and were plotted in the graphs. The error bars indicate standard deviations.

T31N, or Arf1-Q71L together with plasmids expressing RCNMV RNA1 and RNA2. Northern blot analyses showed that the expression of Arf1 reduced the accumulation of viral RNAs by about 25% (Fig. 3D, first and second lanes), whereas the expression of Arf1-T31N or Arf1-Q71L reduced the accumulation of viral RNAs by more than 80% (Fig. 3D, third and fourth lanes). These results suggest that the constitutive-active mutant of Arf1 is insufficient to support the replication of RCNMV RNA but that GDP/GTP cycling of Arf1 is required for viral RNA replication. Taken together, these results strongly suggest that Arf1 plays an essential role in RCNMV RNA replication.

Arf1 is required for the assembly of the viral replicase complex. The replication of (+)RNA viruses proceeds through many steps, including translation of viral replication proteins, formation of the VRC on appropriate intracellular membranes, and viral RNA synthesis (14). To determine which step(s) of RCNMV RNA replication requires Arf1 function, we first tested whether BFA affects the translation of RCNMV RNA1 using an uncapped re-

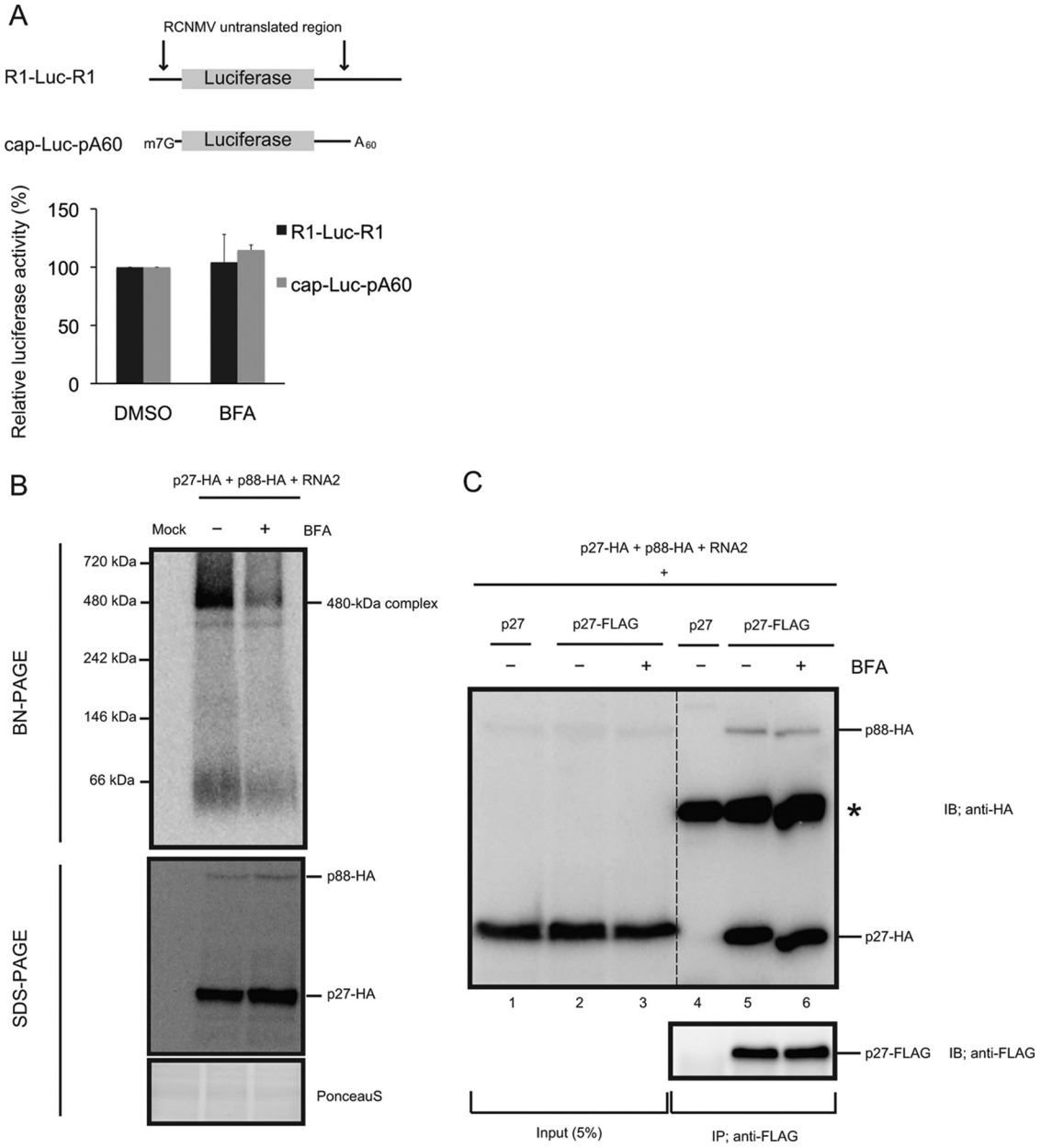

FIG 4 (A) Effects of BFA on RCNMV translation. Tobacco BY-2 protoplasts were inoculated with R1-Luc-R1 and cap-Luc-pA60 in the presence of 10 μg/ml BFA. The luciferase activities of R1-Luc-R1 and cap-Luc-pA60 in the absence of inhibitor were defined as 100%. The error bars indicate standard deviations. (B) Effects of BFA on the accumulation of the 480-kDa replicase complex. RCNMV RNA2 was cotransfected with plasmids expressing p27-HA and p88-HA in BY-2 protoplasts in the presence or absence of 10 μg/ml BFA. After 16 h of incubation, protoplasts were harvested and disrupted by freezing and thawing. Total proteins were extracted from the cell extracts obtained and subjected to BN- and SDS-PAGE analyses, followed by immunoblotting using an anti HA-antibody. Ponceau S staining served as a loading control. (C) BY-2 protoplasts were inoculated with plasmids expressing either p27 or p27-FLAG together with RNA2 and plasmids expressing HA-tagged viral replication proteins in the presence or absence of 10 μg/ml BFA. After 16 h of incubation, protoplasts were harvested and disrupted by freezing and thawing. Subsequently, the cell extracts were subjected to immunoprecipitation using an anti-FLAG antibody. Five percent of the total fraction (lanes 1 to 3) and the eluted fraction (lanes 4 to 6) were subjected to SDS-PAGE and analyzed by immunoblotting (IB) using anti-HA and anti-FLAG antibodies. *, Nonspecific IgG heavy chain.

porter RNA containing the firefly luciferase (Luc) gene flanking the 5′ and 3′ untranslated region (UTR) of the RCNMV RNA1 (R1-Luc-R1) and a capped nonviral reporter Luc RNA with a 3′ poly(A) tail (Luc-pA60) (Fig. 4A) (53, 71). Tobacco BY-2 protoplasts were inoculated with these reporter RNAs and incubated for 6 h in the presence or absence of BFA. Subsequently, luciferase activity was measured. BFA did not affect the translational activity of these RNAs (Fig. 4A), suggesting that BFA affects neither 3′ cap-independent translation element (CITE)-mediated translation of RCNMV RNA nor canonical cap-dependent translation.

Next, we investigated whether BFA affects the formation of the 480-kDa viral RNA replicase complex (29). We expressed C-terminally hemagglutinin (HA)-tagged p27 (p27-HA) and p88 (p88-HA) together with RNA2 in BY-2 protoplasts and analyzed the

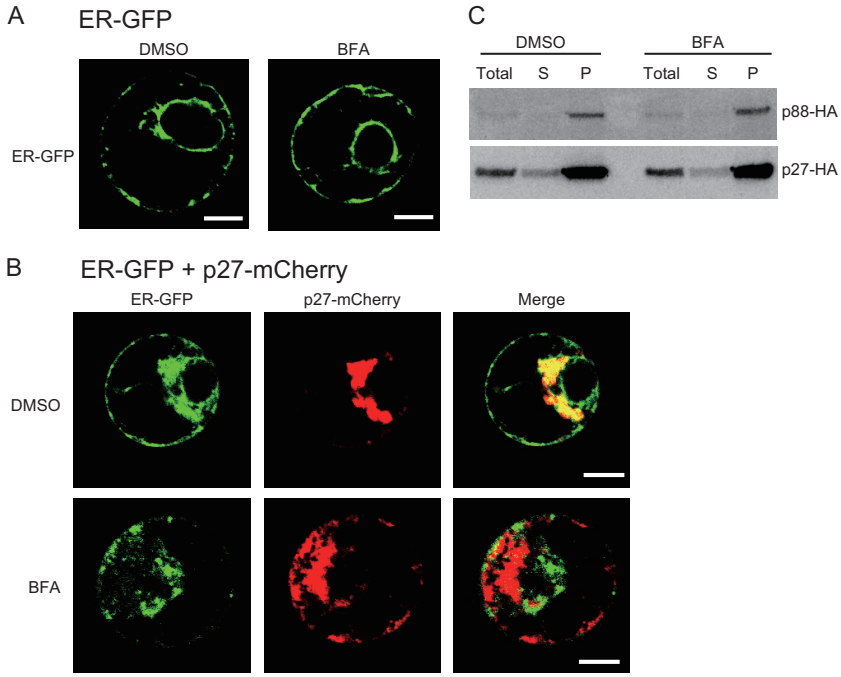

FIG 5 Tobacco BY-2 protoplasts were inoculated with ER-GFP alone (A) or ER-GFP and p27-mCherry (B). BFA (10 μg/ml) was added to protoplasts 2 h before observation. Fluorescence was observed at 16 h postinoculation. The merging of green and red fluorescence is shown in yellow. Scale bars, 5 μm. (C) Immunoblot analyses of RCNMV replication proteins from cellular fractions of tobacco BY-2 protoplasts. Plasmids expressing p27-HA and p88-HA were transfected with RNA2 into BY-2 protoplasts. After 16 h of incubation, protoplasts were harvested, disrupted by freezing and thawing, and centrifuged at 4,000 × *g*. The cell extracts obtained (total fraction) were centrifuged further at 21,000 × *g* to separate the supernatant (S) and pellet (P) fractions. These fractions were separated by SDS-PAGE and visualized using an anti-HA antibody.

accumulation of the viral replicase complexes by SDS- and BN-PAGE using anti-HA antibody. The accumulation of the 480-kDa replicase complex was significantly decreased by BFA treatment (Fig. 4B, upper panel), whereas the accumulation of p27-HA and p88-HA was not affected by BFA (Fig. 4B, lower panel), suggesting that Arf1 is required for the formation of the RCNMV replicase complex.

Because the formation of the 480-kDa complex requires p27-p27/p88 interactions (52, 57), we examined the effect of BFA on the interactions between viral replication proteins. For this, BY-2 protoplasts were transfected with plasmids expressing p27-HA and p88-HA and RNA2 together with either p27 or C-terminally FLAG-tagged p27 (p27-FLAG). After 16 h of incubation in the presence or absence of BFA, cell extracts were subjected to FLAG affinity resin, and eluates were analyzed by immunoblotting using an anti-HA antibody. BFA had no effect on the copurification of either p27-HA or p88-HA by p27-FLAG (Fig. 4C, lanes 5 and 6). p27-HA and p88-HA were not immunoprecipitated with the anti-FLAG antibody (Fig. 4C, lane 4), ruling out the possibility of nonspecific copurification. These results showed that BFA does not prevent the p27-p27/p88 interactions.

Arf function is required for p27-mediated ER modification. Because the membrane association of p27 is critical for the assembly of the 480-kDa replicase complex (30) and because Arf1 is involved in COPI vesicle formation and membrane curvature (72), we investigated whether Arf1 function is required to keep the ER membrane association of p27. For this, BY-2 protoplasts were transfected with a plasmid expressing GFP containing an ER-targeting sequence (ER-GFP) together with or without a plasmid expressing p27-mCherry. Protoplasts were incubated for 14 h, followed by an additional incubation of 2 h with BFA or DMSO. As reported previously (30, 31), p27-mCherry colocalized with ER-GFP in p27-induced large aggregate structures in the DMSO control (Fig. 5B, upper panels). In contrast, BFA treatment canceled the colocalization of p27-mCherry with ER-GFP in protoplasts treated with BFA (Fig. 5B, lower panels). The fluorescence of both ER-GFP and p27-mCherry dispersed in the BFA-treated protoplasts compared with that observed in control protoplasts (Fig. 5B, data not shown). Interestingly, in the absence of p27-mCherry, BFA treatment did not affect the distribution patterns of ER-GFP (Fig. 5A). Moreover, BFA had no effect on the distribution patterns of either p27-HA or p88-HA, as assessed using a fractionation assay (Fig. 5C). These observations suggest that Arf1 is required for p27-mediated ER modification.

Disturbance of COPII vesicle formation inhibits the replication of RCNMV RNA. It is known that BFA treatment or expression of Arf1-T31N not only impairs the normal COPI function but also inhibits COPII vesicle formation (65). COPII vesicles bud from ERES and are thought to mediate anterograde traffic out of the ER (73–75). Sar1 is a small GTPase that is an essential cytosolic component of the COPII complex that accumulates at ERES (76). To examine whether the COPII vesicle transport system is involved in RCNMV RNA replication, we used a dominant negative mutant of Sar1 (Sar1-H74L). Sar1-H74L is the GTP-restricted mutant that exerts a known dominant negative effect on COPII vesicle transport. This mutant was shown previously to trap vesicles in a coated configuration so that they are unable to fuse with the target membrane (58, 73).

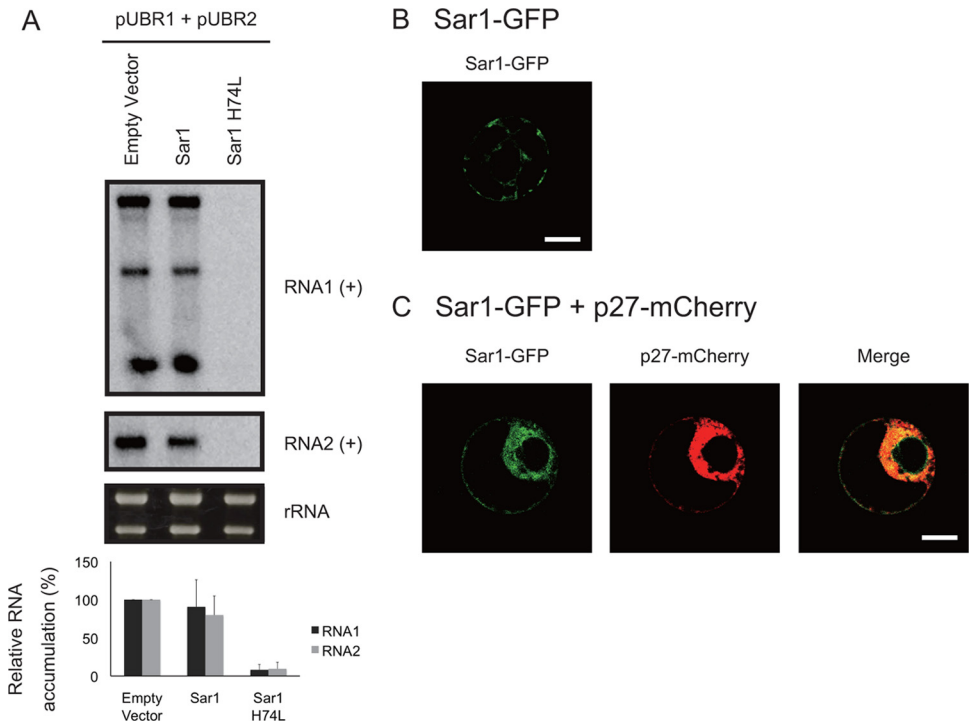

FIG 6 (A) Dominant negative mutants of Sar1 inhibit RCNMV replication. Tobacco BY-2 protoplasts were transfected with plasmids expressing either wild-type Sar1 or Sar1-H74L together with pUBRC1 and pUBRC2. The inoculated protoplasts were incubated at 17°C for 24 h. Total RNA was analyzed by Northern blotting. Ethidium bromide-stained rRNAs were used as loading controls and are shown below the Northern blots. The accumulation levels of RCNMV RNAs from three separate experiments were quantified using the Image Gauge program and were plotted in the graphs. The error bars indicate standard deviations. (B and C) Colocalization of Sar1 with p27. A plasmid expressing C-terminally GFP-fused Sar1 (Sar1-GFP) was cotransfected with either the empty vector or a plasmid expressing C-terminally mCherry-fused p27 (p27-mCherry) into tobacco BY-2 protoplasts. Fluorescence was observed after 16 h of incubation. (B) Localization of Sar1-GFP in the absence of p27-mCherry. (C) Localization of Sar1-GFP in the presence of p27-mCherry. Fluorescence was visualized by confocal microscopy. The merging of green and red fluorescence is shown in yellow. Scale bar, 5 μm.

Tobacco BY-2 protoplasts were transfected with plasmids expressing either wild-type Sar1 or Sar1-H74L together with plasmids expressing RCNMV RNA1 and RNA2, and the accumulation of RNA1 and RNA2 was determined at 24 hpi. Northern blot analyses showed that the expression of Sar1 did not significantly affect the accumulation of viral RNAs (Fig. 6A, first and second lanes). In contrast, the expression of the Sar1-H74L mutant dramatically reduced the accumulations of viral RNAs (Fig. 6A, third lane). The fluorescence of C-terminally GFP-fused Sar1 (Sar1-GFP) was observed as small punctate structures dispersed in cells (Fig. 6B). Interestingly, coexpression of p27-mCherry redistributed Sar1-GFP to perinuclear aggregated structures in which these proteins were well colocalized (Fig. 6C).

RCNMV replication proteins colocalize with newly synthesized viral RNAs. To determine whether newly synthesized RCNMV RNAs colocalized with viral replication proteins, we performed double immunofluorescence staining of RCNMV-infected tobacco BY-2 protoplasts. BY-2 protoplasts were inoculated with RNA1 and RNA2. After 14 h of incubation, protoplasts were incubated with actinomycin D for 1 h to block host DNA-dependent RNA polymerases. Protoplasts were then incubated with BrUTP for an additional 3 h, fixed, and processed for double immunofluorescence labeling using an anti-p27 antiserum and an antibody that recognizes bromouridine-containing RNA. To assess the background fluorescence, mock-inoculated protoplasts were subjected to the same immunofluorescence labeling conditions, and fluorescent signals were adjusted to set the background threshold level. No significant background was detected in uninfected protoplasts (Fig. 7). Immunofluorescence labeling showed that bromouridine-labeled RNA (red) colocalized with p27 (green) (Fig. 7), indicating that RCNMV replication proteins colocalize with newly synthesized viral RNA.

DISCUSSION

In this study, we found that p27 interacts with Arf1 and relocalizes this protein to the aggregate structures of ER membranes, where they colocalize (Fig. 1 and 2), suggesting that p27 recruits Arf1 to the viral replication sites. Membrane remodeling, including the formation of the aggregate structures and membrane proliferation, has been observed in plant cells infected with RCNMV or expressing p27 alone (30–32). Arf1 seems to be required for the formation of virus-induced ER membrane proliferation. Pharmacological inhibition of Arf function by BFA canceled the p27-induced formation of aggregate structures on ER membranes (Fig. 5B). However, BFA treatment did not affect the membrane association of p27 (Fig. 5C) or the localization of ER-GFP, an ER marker in the absence of p27 (Fig. 5A). Moreover, the N-terminal half of p27 interacted poorly with Arf1 (Fig. 1D) but retained the ability to efficiently localize at the ER membrane (30). This truncated p27 mutant does not induce large aggregate structures on ER membranes although it induces smaller punctate structures (30). All these observations strongly support the importance of func-

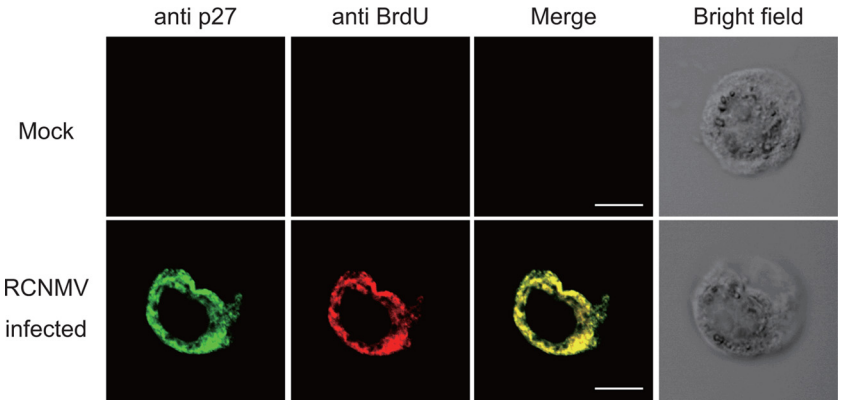

FIG 7 Colocalization of incorporated BrUTP with RCNMV replication proteins. Representative images from mock-inoculated (upper row) or RCNMV-infected (lower row) BY-2 protoplasts incubated for 14 h postinoculation, incubated for an additional 1 h with actinomycin D, labeled with BrUTP, fixed, and processed for double-labeled immunofluorescence using antibodies that recognize p27 (green) and incorporated BrUTP (red). Scale bar, 10 μm.

tional Arf1 in membrane remodeling, such as the induction of a large aggregate structure that is likely the site of vital RNA replication (Fig. 7).

In animal and yeast cells, it is known that membrane-bound Arf1 can recruit a diverse array of effectors, including COPI, clathrin, cytoskeletal regulators, and lipid-modifying enzymes, such as phospholipase D and PI4KIIIβ (77). Arf1 also plays a crucial role in the replication of several vertebrate (+)RNA viruses. Arf1 colocalizes with the enteroviral replication machinery (23, 39) and binds to and hydrolyzes GTP during infection, suggesting the utilization of Arf1 effectors by the virus (78). The enterovirus replication protein 3A recruits PI4KIIIβ, one of the Arf1 effectors, over many other Arf1 effector proteins to membranes (23). Although there is no information regarding the function of Arf1 effector proteins as lipid-modifying enzymes in plant cells (34), plant Arf1 effectors might contribute to the establishment of VRCs of RCNMV via a mechanism similar to that reported in vertebrate viruses (23). Interestingly, we noted that treatment of RCNMV-infected BY-2 protoplasts with 1-butanol, which inhibits the production of phosphatidic acid catalyzed by phospholipase D (79), inhibited the accumulation of viral RNAs (K. Hyodo and T. Okuno, unpublished data). Arf1 appears to manage not only coat recruitment but also curvature generation in membranes (72). After membrane binding, Arf1 can remodel membranes into highly curved tubules *in vitro* (80, 81). The membrane deformation activity of Arf1 *per se* may contribute to the formation of RCNMV VRCs. In the case of BMV, Rhps are recruited to viral RNA replication site by 1a protein to induce the membrane curvature (22).

BFA treatment or expression of dominant negative mutants of Arf1 in plant cells not only inhibits the COPI pathway but also compromises COPII vesicle trafficking (65). Interestingly, we found that the accumulation of RCNMV RNA was inhibited by the expression of the Sar1 H74L mutant (Fig. 6A), which inhibits COPII vesicle formation in plant cells (58, 73). Sar1 was relocalized with p27 in p27-induced large aggregate structures of ER membranes (Fig. 6B and C). These results suggest that the COPII vesicle trafficking system is required for the formation of the RNA replication compartment in RCNMV. The COPII assembly system also plays an important role in MHV and poliovirus replication (82, 83). Poliovirus induces COPII vesicles in the early replication phase, and viral RNA localizes at or near the ERES (23, 83).

The p27-induced remodeling of the early secretory pathway is reminiscent of the membrane remodeling caused by potato virus X (PVX) and turnip mosaic virus (TuMV) infection (84, 85). The triple gene block 1 (TGB1) of PVX organizes the X body, a virally induced inclusion structure that contains host actin, the ER, and the Golgi apparatus, at the perinuclear region (85). However, TGB1 is not required for PVX replication. Therefore, the X body seems to couple RNA replication and cell-to-cell movement processes (85). TuMV infection leads to the amalgamation of the host ER, Golgi apparatus, components of the COPII coatomer, and chloroplasts into a perinuclear globular structure that also contains viral proteins (84). However, the formation of this globular structure is independent of the early secretory pathway (84). In contrast to TuMV, p27-induced membrane remodeling relied on the functional secretory pathway because BFA treatment disrupted this membrane remodeling (Fig. 5). Rearrangement of host endomembrane systems has also been reported in several vertebrate (+)RNA viruses (18). Remodeling of the early secretory pathway may be a common phenomenon during (+)RNA virus infection although the molecular mechanisms underlying its formation may be different in each virus.

BFA inhibits Arf function through BFA-sensitive GEFs, which assist the GDP-GTP exchange reaction of Arf proteins (36, 37). Poliovirus uses Arf1 and GBF1, which is a BFA-sensitive Arf-GEF (40). The poliovirus 3A protein interacts with GBF1 (86). However, it is well known that the replication of several viruses in the *Picornaviridae* is insensitive to BFA (87, 88). Among plant RNA viruses, TuMV, melon necrotic spot virus (MNSV), and BMV were insensitive to BFA during RNA replication (84, 89) (Fig. 3C), whereas grapevine fanleaf virus (90) and RCNMV (Fig. 3) were sensitive to BFA during RNA replication. The BFA-insensitive viruses may require BFA-insensitive GEFs or other host factors involved in the secretory pathway. Recent proteomics analyses suggested that a large number of host proteins involved in protein transport affect TBSV replication (11). Interestingly, downregulation of the COPI coatomer subunit decreases TBSV replication but increases recombination in *Saccharomyces cerevisiae* (5, 91). (+)RNA viruses may evolve to hijack a diverse set of component proteins in the host secretory pathway to accomplish efficient viral infection.

The involvements of the early secretory pathway in the cell-to-cell movement of several plant (+)RNA viruses has been reported

(92). Disruption of the early secretory pathway by BFA treatment or expression of a dominant negative mutant of Arf1 in *N. benthamiana* epidermal cells leads to the inhibition of cell-to-cell movement of TuMV and MNSV, with little effect on viral RNA replication (84, 89). Although inhibition of the early secretory pathway by BFA compromised the RNA replication of RCNMV, it is possible that the early secretory pathway also affects the cell-to-cell movement of RCNMV. Our previous study showed that RCNMV MP localizes to the cell wall and later to the ER (27). Interestingly, the replication of RCNMV RNA1 is coupled to the ER localization of MP (27). p27-induced endomembrane remodeling might contribute not only to VRC formation but also to the recruitment of MP to the VRC and subsequent cell-to-cell movement of RCNMV, which is required for efficient viral spread.

ACKNOWLEDGMENTS

We thank P. Ahlquist, A. Nakano, and J. Wellink for providing the plasmids. We also thank K. Yazaki for technical assistance.

This study was supported by a Grant-in Aid for Scientific Research (A) (22248002) from the Japan Society for the Promotion of Science (JSPS). K.H. is a JSPS research fellow.

REFERENCES

1. **Berger KL, Cooper JD, Heaton NS, Yoon R, Oakland TE, Jordan TX, Mateu G, Grakoui A, Randall G.** 2009. Roles for endocytic trafficking and phosphatidylinositol 4-kinase III alpha in hepatitis C virus replication. Proc. Natl. Acad. Sci. U. S. A. **106**:7577–7582.
2. **Cherry S, Doukas T, Armknecht S, Whelan S, Wang H, Sarnow P, Perrimon N.** 2005. Genome-wide RNAi screen reveals a specific sensitivity of IRES-containing RNA viruses to host translation inhibition. Genes Dev. **19**:445–452.
3. **Cherry S, Kunte A, Wang H, Coyne C, Rawson RB, Perrimon N.** 2006. COPI activity coupled with fatty acid biosynthesis is required for viral replication. PLoS Pathog. **2**:e102. doi:10.1371/journal.ppat.0020102.
4. **Gancarz BL, Hao L, He Q, Newton MA, Ahlquist P.** 2011. Systematic identification of novel, essential host genes affecting bromovirus RNA replication. PLoS One **6**:e23988. doi:10.1371/journal.pone.0023988.
5. **Jiang Y, Serviene E, Gal J, Panavas T, Nagy PD.** 2006. Identification of essential host factors affecting tombusvirus RNA replication based on the yeast Tet promoters Hughes Collection. J. Virol. **80**:7394–7404.
6. **Kushner DB, Lindenbach BD, Grdzelishvili VZ, Noueiry AO, Paul SM, Ahlquist P.** 2003. Systematic, genome-wide identification of host genes affecting replication of a positive-strand RNA virus. Proc. Natl. Acad. Sci. U. S. A. **100**:15764–15769.
7. **Li Z, Pogany J, Panavas T, Xu K, Esposito AM, Kinzy TG, Nagy PD.** 2009. Translation elongation factor 1A is a component of the tombusvirus replicase complex and affects the stability of the p33 replication co-factor. Virology **385**:245–260.
8. **Panavas T, Serviene E, Brasher J, Nagy PD.** 2005. Yeast genome-wide screen reveals dissimilar sets of host genes affecting replication of RNA viruses. Proc. Natl. Acad. Sci. U. S. A. **102**:7326–7331.
9. **Reiss S, Rebhan I, Backes P, Romero-Brey I, Erfle H, Matula P, Kaderali L, Poenisch M, Blankenburg H, Hiet MS, Longerich T, Diehl S, Ramirez F, Balla T, Rohr K, Kaul A, Bühler S, Pepperkok R, Lengauer T, Albrecht M, Eils R, Schirmacher P, Lohmann V, Bartenschlager R.** 2011. Recruitment and activation of a lipid kinase by hepatitis C virus NS5A is essential for integrity of the membranous replication compartment. Cell Host Microbe **9**:32–45.
10. **Serva S, Nagy PD.** 2006. Proteomics analysis of the tombusvirus replicase: Hsp70 molecular chaperone is associated with the replicase and enhances viral RNA replication. J. Virol. **80**:2162–2169.
11. **Shah Nawaz-ul-Rehman M, Martinez-Ochoa N, Pascal H, Sasvari Z, Herbst C, Xu K, Baker J, Sharma M, Herbst A, Nagy PD.** 2012. Proteome-wide overexpression of host proteins for identification of factors affecting tombusvirus RNA replication: an inhibitory role of protein kinase C. J. Virol. **86**:9384–9395.
12. **Tai AW, Benita Y, Peng LF, Kim SS, Sakamoto N, Xavier RJ, Chung RT.** 2009. A functional genomic screen identifies cellular cofactors of hepatitis C virus replication. Cell Host Microbe **5**:298–307.
13. **Zhu J, Gopinath K, Murali A, Yi G, Hayward SD, Zhu H, Kao C.** 2007. RNA-binding proteins that inhibit RNA virus infection. Proc. Natl. Acad. Sci. U. S. A. **104**:3129–3134.
14. **Nagy PD, Pogany J.** 2012. The dependence of viral RNA replication on co-opted host factors. Nat. Rev. Microbiol. **10**:137–149.
15. **den Boon JA, Ahlquist P.** 2010. Organelle-like membrane compartmentalization of positive-strand RNA virus replication factories. Annu. Rev. Microbiol. **64**:241–256.
16. **den Boon JA, Diaz A, Ahlquist P.** 2010. Cytoplasmic viral replication complexes. Cell Host Microbe **8**:77–85.
17. **Laliberté JF, Sanfaçon H.** 2010. Cellular remodeling during plant virus infection. Annu. Rev. Phytopathol. **48**:69–91.
18. **Miller S, Krijnse-Locker J.** 2008. Modification of intracellular membrane structures for virus replication. Nat. Rev. Microbiol. **6**:363–374.
19. **Barajas D, Jiang Y, Nagy PD.** 2009. A unique role for the host ESCRT proteins in replication of Tomato bushy stunt virus. PLoS Pathog. **5**:e1000705. doi:10.1371/journal.ppat.1000705.
20. **Barajas D, Nagy PD.** 2010. Ubiquitination of tombusvirus p33 replication protein plays a role in virus replication and binding to the host Vps23p ESCRT protein. Virology **397**:358–368.
21. **Reyes FC, Buono R, Otegui MS.** 2011. Plant endosomal trafficking pathways. Curr. Opin. Plant Biol. **14**:666–673.
22. **Diaz A, Wang X, Ahlquist P.** 2010. Membrane-shaping host reticulon proteins play crucial roles in viral RNA replication compartment formation and function. Proc. Natl. Acad. Sci. U. S. A. **107**:16291–16296.
23. **Hsu NY, Ilnytska O, Belov G, Santiana M, Chen YH, Takvorian PM, Pau C, van der Schaar H, Kaushik-Basu N, Balla T, Cameron CE, Ehrenfeld E, van Kuppeveld FJ, Altan-Bonnet N.** 2010. Viral reorganization of the secretory pathway generates distinct organelles for RNA replication. Cell **141**:799–811.
24. **Tai AW, Salloum S.** 2011. The role of the phosphatidylinositol 4-kinase PI4KA in hepatitis C virus-induced host membrane rearrangement. PLoS One **6**:e26300. doi:10.1371/journal.pone.0026300.
25. **Xiong Z, Kim KH, Kendall TL, Lommel SA.** 1993. Synthesis of the putative red clover necrotic mosaic virus RNA polymerase by ribosomal frameshifting in vitro. Virology **193**:213–221.
26. **Xiong Z, Lommel SA.** 1989. The complete nucleotide sequence and genome organization of red clover necrotic mosaic virus RNA-1. Virology **171**:543–554.
27. **Kaido M, Tsuno Y, Mise K, Okuno T.** 2009. Endoplasmic reticulum targeting of the Red clover necrotic mosaic virus movement protein is associated with the replication of viral RNA1 but not that of RNA2. Virology **395**:232–242.
28. **Xiong Z, Kim KH, Giesman-Cookmeyer D, Lommel SA.** 1993. The roles of the red clover necrotic mosaic virus capsid and cell-to-cell movement proteins in systemic infection. Virology **192**:27–32.
29. **Mine A, Takeda A, Taniguchi T, Taniguchi H, Kaido M, Mise K, Okuno T.** 2010. Identification and characterization of the 480-kilodalton template-specific RNA-dependent RNA polymerase complex of red clover necrotic mosaic virus. J. Virol. **84**:6070–6081.
30. **Kusumanegara K, Mine A, Hyodo K, Kaido M, Mise K, Okuno T.** 2012. Identification of domains in p27 auxiliary replicase protein essential for its association with the endoplasmic reticulum membranes in Red clover necrotic mosaic virus. Virology **433**:131–141.
31. **Turner KA, Sit TL, Callaway AS, Allen NS, Lommel SA.** 2004. Red clover necrotic mosaic virus replication proteins accumulate at the endoplasmic reticulum. Virology **320**:276–290.
32. **Mine A, Hyodo K, Tajima Y, Kusumanegara K, Taniguchi T, Kaido M, Mise K, Taniguchi H, Okuno T.** 2012. Differential roles of Hsp70 and Hsp90 in the assembly of the replicase complex of a positive-strand RNA plant virus. J. Virol. **86**:12091–12104.
33. **D'Souza-Schorey C, Chavrier P.** 2006. ARF proteins: roles in membrane traffic and beyond. Nat. Rev. Mol. Cell Biol. **7**:347–358.
34. **Memon AR.** 2004. The role of ADP-ribosylation factor and SAR1 in vesicular trafficking in plants. Biochim. Biophys. Acta **1664**:9–30.
35. **Nebenführ A, Ritzenthaler C, Robinson DG.** 2002. Brefeldin A: deciphering an enigmatic inhibitor of secretion. Plant Physiol. **130**:1102–1108.
36. **Geldner N, Anders N, Wolters H, Keicher J, Kornberger W, Muller P, Delbarre A, Ueda T, Nakano A, Jürgens G.** 2003. The *Arabidopsis* GNOM ARF-GEF mediates endosomal recycling, auxin transport, and auxin-dependent plant growth. Cell **112**:219–230.
37. **Teh OK, Moore I.** 2007. An ARF-GEF acting at the Golgi and in selective endocytosis in polarized plant cells. Nature **448**:493–496.

38. **Mossessova E, Corpina RA, Goldberg J.** 2003. Crystal structure of ARF1*Sec7 complexed with Brefeldin A and its implications for the guanine nucleotide exchange mechanism. Mol. Cell **12**:1403–1411.
39. **Belov GA, Altan-Bonnet N, Kovtunovych G, Jackson CL, Lippincott-Schwartz J, Ehrenfeld E.** 2007. Hijacking components of the cellular secretory pathway for replication of poliovirus RNA. J. Virol. **81**:558–567.
40. **Belov GA, Feng Q, Nikovics K, Jackson CL, Ehrenfeld E.** 2008. A critical role of a cellular membrane traffic protein in poliovirus RNA replication. PLoS Pathog. **4**:e1000216. doi:10.1371/journal.ppat.1000216.
41. **Belov GA, Kovtunovych G, Jackson CL, Ehrenfeld E.** 2010. Poliovirus replication requires the N terminus but not the catalytic Sec7 domain of ArfGEF GBF1. Cell Microbiol. **12**:1463–1479.
42. **Cuconati A, Molla A, Wimmer E.** 1998. Brefeldin A inhibits cell-free, de novo synthesis of poliovirus. J. Virol. **72**:6456–6464.
43. **Goueslain L, Alsaleh K, Horellou P, Roingeard P, Descamps V, Duverlie G, Ciczora Y, Wychowski C, Dubuisson J, Rouillé Y.** 2010. Identification of GBF1 as a cellular factor required for hepatitis C virus RNA replication. J. Virol. **84**:773–787.
44. **Lanke KH, van der Schaar HM, Belov GA, Feng Q, Duijsings D, Jackson CL, Ehrenfeld E, van Kuppeveld FJ.** 2009. GBF1, a guanine nucleotide exchange factor for Arf, is crucial for coxsackievirus B3 RNA replication. J. Virol. **83**:11940–11949.
45. **Matto M, Sklan EH, David N, Melamed-Book N, Casanova JE, Glenn JS, Aroeti B.** 2011. Role for ADP ribosylation factor 1 in the regulation of hepatitis C virus replication. J. Virol. **85**:946–956.
46. **Verheije MH, Raaben M, Mari M, Te Lintelo EG, Reggiori F, van Kuppeveld FJ, Rottier PJ, de Haan CA.** 2008. Mouse hepatitis coronavirus RNA replication depends on GBF1-mediated ARF1 activation. PLoS Pathog. **4**:e1000088. doi:10.1371/journal.ppat.1000088.
47. **Verchot J.** 2011. Wrapping membranes around plant virus infection. Curr. Opin. Virol. **1**:388–395.
48. **Takeda A, Tsukuda M, Mizumoto H, Okamoto K, Kaido M, Mise K, Okuno T.** 2005. A plant RNA virus suppresses RNA silencing through viral RNA replication. EMBO J. **24**:3147–3157.
49. **Xiong ZG, Lommel SA.** 1991. Red clover necrotic mosaic virus infectious transcripts synthesized in vitro. Virology **182**:388–392.
50. **Janda M, French R, Ahlquist P.** 1987. High efficiency T7 polymerase synthesis of infectious RNA from cloned brome mosaic virus cDNA and effects of 5′ extensions on transcript infectivity. Virology **158**:259–262.
51. **Kaido M, Funatsu N, Tsuno Y, Mise K, Okuno T.** 2011. Viral cell-to-cell movement requires formation of cortical punctate structures containing Red clover necrotic mosaic virus movement protein. Virology **413**:205–215.
52. **Hyodo K, Mine A, Iwakawa HO, Kaido M, Mise K, Okuno T.** 2011. Identification of amino acids in auxiliary replicase protein p27 critical for its RNA-binding activity and the assembly of the replicase complex in Red clover necrotic mosaic virus. Virology **413**:300–309.
53. **Sarawaneeyaruk S, Iwakawa HO, Mizumoto H, Murakami H, Kaido M, Mise K, Okuno T.** 2009. Host-dependent roles of the viral 5′ untranslated region (UTR) in RNA stabilization and cap-independent translational enhancement mediated by the 3′ UTR of Red clover necrotic mosaic virus RNA1. Virology **391**:107–118.
54. **Mizumoto H, Tatsuta M, Kaido M, Mise K, Okuno T.** 2003. Cap-independent translational enhancement by the 3′ untranslated region of red clover necrotic mosaic virus RNA1. J. Virol. **77**:12113–12121.
55. **Coemans B, Takahashi Y, Berberich T, Ito A, Kanzaki H, Matsumura H, Saitoh H, Tsuda S, Kamoun S, Sági L, Swennen R, Terauchi R.** 2008. High-throughput in planta expression screening identifies an ADP-ribosylation factor (ARF1) involved in non-host resistance and R gene-mediated resistance. Mol. Plant Pathol. **9**:25–36.
56. **Ratcliff F, Martin-Hernandez AM, Baulcombe DC.** 2001. Technical advance. Tobacco rattle virus as a vector for analysis of gene function by silencing. Plant J. **25**:237–245.
57. **Mine A, Hyodo K, Takeda A, Kaido M, Mise K, Okuno T.** 2010. Interactions between p27 and p88 replicase proteins of Red clover necrotic mosaic virus play an essential role in viral RNA replication and suppression of RNA silencing via the 480-kDa viral replicase complex assembly. Virology **407**:213–224.
58. **Takeuchi M, Ueda T, Sato K, Abe H, Nagata T, Nakano A.** 2000. A dominant negative mutant of Sar1 GTPase inhibits protein transport from the endoplasmic reticulum to the Golgi apparatus in tobacco and *Arabidopsis* cultured cells. Plant J. **23**:517–525.
59. **Carette JE, Stuiver M, Van Lent J, Wellink J, Van Kammen A.** 2000. Cowpea mosaic virus infection induces a massive proliferation of endoplasmic reticulum but not Golgi membranes and is dependent on *de novo* membrane synthesis. J. Virol. **74**:6556–6563.
60. **Taniguchi T, Kido S, Yamauchi E, Abe M, Matsumoto T, Taniguchi H.** 2010. Induction of endosomal/lysosomal pathways in differentiating osteoblasts as revealed by combined proteomic and transcriptomic analyses. FEBS Lett. **584**:3969–3974.
61. **Laemmli UK.** 1970. Cleavage of structural proteins during the assembly of the head of bacteriophage T4. Nature **227**:680–685.
62. **Komoda K, Naito S, Ishikawa M.** 2004. Replication of plant RNA virus genomes in a cell-free extract of evacuolated plant protoplasts. Proc. Natl. Acad. Sci. U. S. A. **101**:1863–1867.
63. **Cui X, Wei T, Chowda-Reddy RV, Sun G, Wang A.** 2010. The Tobacco etch virus P3 protein forms mobile inclusions via the early secretory pathway and traffics along actin microfilaments. Virology **397**:56–63.
64. **Lee MH, Min MK, Lee YJ, Jin JB, Shin DH, Kim DH, Lee KH, Hwang I.** 2002. ADP-ribosylation factor 1 of *Arabidopsis* plays a critical role in intracellular trafficking and maintenance of endoplasmic reticulum morphology in Arabidopsis. Plant Physiol. **129**:1507–1520.
65. **Stefano G, Renna L, Chatre L, Hanton SL, Moreau P, Hawes C, Brandizzi F.** 2006. In tobacco leaf epidermal cells, the integrity of protein export from the endoplasmic reticulum and of ER export sites depends on active COPI machinery. Plant J. **46**:95–110.
66. **Takeuchi M, Ueda T, Yahara N, Nakano A.** 2002. Arf1 GTPase plays roles in the protein traffic between the endoplasmic reticulum and the Golgi apparatus in tobacco and Arabidopsis cultured cells. Plant J. **31**:499–515.
67. **Boevink P, Oparka K, Santa Cruz S, Martin B, Betteridge A, Hawes C.** 1998. Stacks on tracks: the plant Golgi apparatus traffics on an actin/ER network. Plant J. **15**:441–447.
68. **Nebenführ A, Gallagher LA, Dunahay TG, Frohlick JA, Mazurkiewicz AM, Meehl JB, Staehelin LA.** 1999. Stop-and-go movements of plant Golgi stacks are mediated by the acto-myosin system. Plant Physiol. **121**:1127–1142.
69. **Saint-Jore CM, Evins J, Batoko H, Brandizzi F, Moore I, Hawes C.** 2002. Redistribution of membrane proteins between the Golgi apparatus and endoplasmic reticulum in plants is reversible and not dependent on cytoskeletal networks. Plant J. **29**:661–678.
70. **Xu J, Scheres B.** 2005. Dissection of *Arabidopsis* ADP-ribosylation factor 1 function in epidermal cell polarity. Plant Cell **17**:525–536.
71. **Iwakawa HO, Tajima Y, Taniguchi T, Kaido M, Mise K, Tomari Y, Taniguchi H, Okuno T.** 2012. Poly(A)-binding protein facilitates translation of an uncapped/nonpolyadenylated viral RNA by binding to the 3′ untranslated region. J. Virol. **86**:7836–7849.
72. **Pucadyil TJ, Schmid SL.** 2009. Conserved functions of membrane active GTPases in coated vesicle formation. Science **325**:1217–1220.
73. **daSilva LL, Snapp EL, Denecke J, Lippincott-Schwartz J, Hawes C, Brandizzi F.** 2004. Endoplasmic reticulum export sites and Golgi bodies behave as single mobile secretory units in plant cells. Plant Cell **16**:1753–1771.
74. **Marti L, Fornaciari S, Renna L, Stefano G, Brandizzi F.** 2010. COPII-mediated traffic in plants. Trends Plant Sci. **15**:522–528.
75. **Yang YD, Elamawi R, Bubeck J, Pepperkok R, Ritzenthaler C, Robinson DG.** 2005. Dynamics of COPII vesicles and the Golgi apparatus in cultured *Nicotiana tabacum* BY-2 cells provides evidence for transient association of Golgi stacks with endoplasmic reticulum exit sites. Plant Cell **17**:1513–1531.
76. **Hanton SL, Chatre L, Matheson LA, Rossi M, Held MA, Brandizzi F.** 2008. Plant Sar1 isoforms with near-identical protein sequences exhibit different localisations and effects on secretion. Plant Mol. Biol. **67**:283–294.
77. **Donaldson JG, Jackson CL.** 2011. ARF family G proteins and their regulators: roles in membrane transport, development and disease. Nat. Rev. Mol. Cell Biol. **12**:362–375.
78. **Altan-Bonnet N, Balla T.** 2012. Phosphatidylinositol 4-kinases: hostages harnessed to build panviral replication platforms. Trends Biochem. Sci. **37**:293–302.
79. **Brown HA, Gutowski S, Moomaw CR, Slaughter C, Sternweis PC.** 1993. ADP-ribosylation factor, a small GTP-dependent regulatory protein, stimulates phospholipase D activity. Cell **75**:1137–1144.
80. **Beck R, Sun Z, Adolf F, Rutz C, Bassler J, Wild K, Sinning I, Hurt E, Brügger B, Bëthune J, Wieland F.** 2008. Membrane curvature induced by

Arf1-GTP is essential for vesicle formation. Proc. Natl. Acad. Sci. U. S. A. **105**:11731–11736.
81. **Krauss M, Jia JY, Roux A, Beck R, Wieland FT, De Camilli P, Haucke V.** 2008. Arf1-GTP-induced tubule formation suggests a function of Arf family proteins in curvature acquisition at sites of vesicle budding. J. Biol. Chem. **283**:27717–27723.
82. **Oostra M, te Lintelo EG, Deijs M, Verheije MH, Rottier PJ, de Haan CA.** 2007. Localization and membrane topology of coronavirus nonstructural protein 4: involvement of the early secretory pathway in replication. J. Virol. **81**:12323–12336.
83. **Trahey M, Oh HS, Cameron CE, Hay JC.** 2012. Poliovirus infection transiently increases COPII vesicle budding. J. Virol. **86**:9675–9682.
84. **Grangeon R, Agbeci M, Chen J, Grondin G, Zheng H, Laliberté JF.** 2012. Impact on the endoplasmic reticulum and Golgi apparatus of turnip mosaic virus infection. J. Virol. **86**:9255–9265.
85. **Tilsner J, Linnik O, Wright KM, Bell K, Roberts AG, Lacomme C, Santa Cruz S, Oparka KJ.** 2012. The TGB1 movement protein of Potato virus X reorganizes actin and endomembranes into the X-body, a viral replication factory. Plant Physiol. **158**:1359–1370.
86. **Teterina NL, Pinto Y, Weaver JD, Jensen KS, Ehrenfeld E.** 2011. Analysis of poliovirus protein 3A interactions with viral and cellular proteins in infected cells. J. Virol. **85**:4284–4296.
87. **Irurzun A, Perez L, Carrasco L.** 1992. Involvement of membrane traffic in the replication of poliovirus genomes: effects of brefeldin A. Virology **191**:166–175.
88. **Sasaki J, Ishikawa K, Arita M, Taniguchi K.** 2012. ACBD3-mediated recruitment of PI4KB to picornavirus RNA replication sites. EMBO J. **31**:754–766.
89. **Genovés A, Navarro JA, Pallás V.** 2010. The intra- and intercellular movement of Melon necrotic spot virus (MNSV) depends on an active secretory pathway. Mol. Plant Microbe Interact. **23**:263–272.
90. **Ritzenthaler C, Laporte C, Gaire F, Dunoyer P, Schmitt C, Duval S, Piéquet A, Loudes AM, Rohfritsch O, Stussi-Garaud C, Pfeiffer P.** 2002. Grapevine fanleaf virus replication occurs on endoplasmic reticulum-derived membranes. J. Virol. **76**:8808–8819.
91. **Serviene E, Jiang Y, Cheng CP, Baker J, Nagy PD.** 2006. Screening of the yeast yTHC collection identifies essential host factors affecting tombusvirus RNA recombination. J. Virol. **80**:1231–1241.
92. **Harries PA, Schoelz JE, Nelson RS.** 2010. Intracellular transport of viruses and their components: utilizing the cytoskeleton and membrane highways. Mol. Plant Microbe Interact. **23**:1381–1393.